Desalination and Water Treatment
www.deswater.com

doi: 10.1080/19443994.2016.1141373

57 (2016) 24257–24266
November

Taylor & Francis
Taylor & Francis Group

Numerical simulation of additional guiding baffles to improve velocity distribution in an oxidation ditch

Wenli Wei*, Zewei Zhang, Yan Zheng, Yuling Liu

State Key Laboratory base of Eco-Hydraulic Engineering in Arid Area (SKLEHE), Xi'an University of Technology, Xi'an, Shaanxi 710048, China, Tel. +86 15596886263; email: wei_wenli@126.com (W. Wei), Tel. +86 15191913820; email: Zewei@126.com (Z. Zhang), Tel. +86 13991987708; email: Zhengyan@126.com (Y. Zhen), Tel. +86 18591999882; email: liuyuling@xaut.edu.cn (Y. Liu)

Received 1 April 2015; Accepted 3 January 2016

ABSTRACT

The effect of guiding baffles downstream from surface aerators on the flow fields in an oxidation ditch (OD) was studied using an experimentally validated numerical tool, based on computational fluid dynamics (CFD) model. The two-phase gas–liquid model and the 3D RNG k-ε turbulence model were used to describe flow motion in ODs. The algorithm of pressure-implicit with splitting of operators (PISO) was used to solve velocity and pressure. The volume of fluid (VOF) method was used to simulate free water surface. Comparisons of the velocity distributions under the two conditions (with and without guiding baffles) show that the installed guiding baffles downstream from the surface aerators can increase the velocity at the ditch bottom, and the vertical velocity distributions in the OD become more uniform, which will help to prevent sludge deposit at the bottom of an OD and have an obvious effect on time prolongation for liquid–gas mixture.

Keywords: Oxidation ditch; Numerical simulation; Guiding baffles; Turbulence

1. Introduction

OD is an improved activated sludge treatment process, and plays an important role in the city sewage and industrial wastewater treatment system [1,2]. The hydraulic characteristics of an OD have a significant effect on the efficiency of wastewater treatment for the OD; therefore, many scholars have put forward some measures to improve it with simulation and experimental methods. Cao and Fu [3] did an experiment about an OD, by which he put forward that installing guiding baffles upstream and downstream from the surface aerators can improve the velocity distribution, and eliminate sludge deposit at the bottom. Zhao [4] proposed a calculation formula for the relationship between the water head lifting and loss in an OD, and also put forward that tilted guiding baffles can prevent sludge deposit in the bend ditches. Yang et al. [5] discussed the influence of the installation position and the submerged depth of surface aerators on the dissolved oxygen concentration distribution. With the development of computer technology and calculation method, CFD has been widely used in the study of ODs. Li et al. [6] simulated the flows of an OD with and without guiding plate downstream from surface aerators with the realizable κ–ε model, by which they put forward the reasonable parameters for the installation of guiding baffles. Oda et al. [7] used the

*Corresponding author.

3D multiphase flow turbulent model along with the microbial reaction model, sludge settling model, coarse bubble oxygen transfer model, and micro bubble oxygen transfer model to analyze the biological reaction and sludge flowing process. Chen and Yang [8] proposed a corrugated baffle as a division wall for an OD, which can reduce the region of low velocity and prevent the sludge deposition. Simon et al. [9] developed a theoretical model based on the quality and momentum balance to predict the velocity field in a test device, and the simulation results agree well with the experimental data. Song et al. [10] modeled the flow field in an OD, and obtained the velocity distribution in the straight channels, and the formation and development of the cross-sectional circulations in the bends. Tang et al. [11] used the RNG κ–ε model to simulate the 3D flow field driven by submerged impellers based on the multiple reference frame (MRF) defining the impellers' rotation, which shows that the mathematical model can accurately simulate the 3Dflow field. Yang et al. [12] used a new method called moving wall model to optimize the flow field in a full-scale Carrousel OD with many sets of disk aerators operating simultaneously. Xie et. al [13] proposed a two-phase (liquid–solid) CFD model for simulating the flow field and sludge settling in a full-scale Carrousel OD, and applied the Takács double exponential sedimentation velocity function to simulate the two-phase flow. Based on the simulation results of the flow field and sludge settling using this two-phase CFD model, an optimized operation scheme of the OD was proposed. Lei and Ni [14] developed a three-dimensional three-phase fluid model, supplemented by laboratory data, to simulate the hydrodynamics, oxygen mass transfer, carbon oxidation, nitrification, and denitrification processes in an OD. Floc parameters were modified to improve the sludge viscosity, sludge density, oxygen mass transfer rate, and carbon substrate uptake due to adsorption onto the activated sludge. The validation test results were in very satisfactory agreement with laboratory data on the behavior of activated sludge in an OD.

Generally, in an OD, aeration and mixing are promoted by ensuring that horizontal velocity (HV) in the reactor is sufficient to create suitable turbulence [15]. Thus, HV between 0.25 and 0.60 m/s with a typical value between 0.25 and 0.35 m/s is an important factor in an OD for better operation [16,17]. An HV more than 0.25 m/s is usually recommended to supply a sufficient quantity of dissolved oxygen (DO) to maintain aerobic conditions and avoid anaerobic zones, and to prevent the settling of organic and solid particles [16,18,19].

In order to prevent the sludge deposition, the mixture should have a certain range of velocity; generally, it is believed that the section-averaged velocity of an OD is no less than 0.3 m/s, and the bottom velocity is more than 0.15 m/s [20]. It is noted that in recent years, with an increase in the water depth of an OD, the velocity of upper flow near water surface becomes larger, and that of the lower flow near bottom becomes too smaller, which makes the above required velocity not be satisfied, and results in sludge deposition at the bottom. If the sets of surface aerators cannot support enough energy source to meet the above requirement of flow velocity, additional submerged impellers are necessarily required; still, additional guiding baffles can improve the vertical distribution of flow velocity. The objective of this paper is that we added guiding baffles downstream from surface aerators to promote flow fields, and used the CFD package FLUENT 6.2.16 to simulate the effect of added guiding baffles on improving the vertical distribution of flow velocities in an OD.

2. Mathematical model

2.1. Governing equations

The unsteady 3D flow governing equations for continuity, momentum can be written as follows [20,21]:

Continuity equation:

$$\frac{\partial \rho}{\partial t} + \frac{\partial (\rho u_i)}{\partial x_i} = 0 \tag{1}$$

Momentum equation:

$$\frac{\partial (\rho u_i)}{\partial t} + \frac{\partial (\rho u_i u_j)}{\partial x_j} = -\frac{\partial p}{\partial x_i} + \frac{\partial}{\partial x_j}\left[\mu\left(\frac{\partial u_i}{\partial x_j} + \frac{\partial u_j}{\partial x_i}\right)\right] - \frac{\partial}{\partial x_j}\left(\rho \overline{u_i' u_j'}\right) + \rho g_i \tag{2}$$

where t is density (in water t is equal to the water density; in air t is equal to the air density); t is the time; x_i is the space coordinate in i-direction; p is the pressure; t is the molecular kinematic viscosity; g_i is the gravitational acceleration in i-direction; u_i is the velocity component in i-direction; t and u_j' are the fluctuating velocity components in i- and j-directions, respectively; the subscripts i, $j = 1, 2, 3$; and $-\rho\overline{u_i' u_j'}$ is the Reynolds stress tensor.

The 3D Reynolds-averaged Navier–Stokes equations were closed by the RNG k–ε model, which was

developed using renormalization group (RNG) methods by Yakhot et al. to renormalize the Navier–Stokes equations, to account for the effects of smaller scales of motion [22]. Some workers claim that it offers improved accuracy in rotating flows [23]. The flow in an OD is a bend streamline flow, so the RNG k–ε turbulence model was used here. The formulas for the RNG k–ε turbulence model are given as [20,21]:

$$\frac{\partial(\rho k)}{\partial t}+\frac{\partial(\rho k u_i)}{\partial x_i}=\frac{\partial}{\partial x_j}\left[\left(\mu+\frac{\mu_t}{\sigma_k}\right)\frac{\partial k}{\partial x_j}\right]+P_k-\rho\varepsilon \tag{3}$$

$$\frac{\partial(\rho\varepsilon)}{\partial t}+\frac{\partial(\rho\varepsilon u_i)}{\partial x_i}=\frac{\partial}{\partial x_j}\left[\left(\mu+\frac{\mu_t}{\sigma_\varepsilon}\right)\frac{\partial \varepsilon}{\partial x_j}\right]+C_1\frac{\varepsilon}{k}P_k-\rho C_2\frac{\varepsilon^2}{k} \tag{4}$$

$$\mu_t=\rho C_\mu\frac{k^2}{\varepsilon} \tag{5}$$

$$-\rho\overline{u_i'u_j'}=\mu_t\left(\frac{\partial u_i}{\partial x_j}+\frac{\partial u_j}{\partial x_i}\right)-\frac{2}{3}\left(\rho k+\mu_t\frac{\partial u_i}{\partial x_i}\right)\delta_{ij} \tag{6}$$

where k is the turbulent kinetic energy; ε is the kinetic energy dissipation rate; $P_k=\mu_t(\frac{\partial u_i}{\partial x_j}+\frac{\partial u_j}{\partial x_i})\frac{\partial u_i}{\partial x_j}$ is the production term; δ_{ij} is the Kronecker function, $\delta_{ij}=1$ with $i=j$, and $\delta_{ij}=0$ with $i\neq j$;C_μ, σ_k, C_2 and σ_ε are empirical constants and have the values 0.0845, 0.7179, 1.68, and 0.7179, respectively; and other parameters are: $C_1=1.42-\frac{\widetilde{\eta}(1-\widetilde{\eta}/\widetilde{\eta}_0)}{1+\beta\eta^3}$, $\widetilde{\eta}=Sk/\varepsilon$, $S=(2S_{i,j}S_{i,j})^{1/2}$, $\widetilde{\eta}_0=4.38$, $\beta=0.015$, $S_{i,j}=\frac{1}{2}(\frac{\partial u_i}{\partial x_j}+\frac{\partial u_j}{\partial x_i})$.

In the RNG k–ε model, the modeled transport equations for k and t determine the eddy viscosity, and the Newtonian model (6) provides the Reynolds stress tensor appearing in the Reynolds-averaged Nervier–Stokes Eq. (2) to complete its closure.

2.2. VOF method

To describe the liquid/gas interface, the VOF method [20,21] was used. The volume of water inside a cell, V_w, is computed as $V_w=F\times V_c$, where V_c is the volume of the cell, and F is the liquid volume fraction in the cell, which is defined as the ratio of the volume occupied by liquid in a cell to the total volume of the cell. The value of F in a cell should range between 1 and 0. $F=1$ represents a cell completely filled with liquid, $F=0$ represents a cell completely filled with gas, and $0<F<1$ represents the liquid/gas interface. The liquid volume fraction distribution can be determined by solving the equation given as:

$$\frac{\partial F}{\partial t}+\frac{\partial(Fu_i)}{\partial x_i}=0 \tag{7}$$

The physical properties of the mixture are derived from those of water and air through the volume fraction function. In particular, the average values of ρ and μ in a computational cell can be computed from the value of F in accordance with:

$$\rho=(1-F)\rho_a+F\mu_w \tag{8}$$

$$\mu=(1-F)\mu_a+F\mu_w \tag{9}$$

where ρ_a and μ_a are the density and viscosity of air, respectively; and ρ_w and μ_w are the density and viscosity of water, respectively.

3. Test model and boundary conditions

3.1 Test model size of a Carrousel OD with six channels

The test model made of organic glass is a Carrousel OD with six channels, having a length of 0.85 m, a width of 0.6 m, and a height of 0.16 m, as shown in Fig. 1(a). The six straight channels are labeled as 1~6, respectively, each of which has a width of 0.1 m. The effective water depth is 0.11 m. Three submerged impellers with a diameter of 0.06 m are installed at the centers of the three bends, respectively; and the distance from the installation center to the ditch bottom is 0.055 m. The three surface 0.08 m diameter aerators are installed in no. 1, 3, and 5 channels. The axial length of the surface aerators is 0.1 m. The vertical distance from the axis to the ditch bottom is 0.11 m. The horizontal distance from the axis to the right end of the straight division plate is 0.325 m. The submerged depth of the surface aerators is 0.04 m. The 3D region of the Carrousel OD is shown in Fig. 1(b).

3.2 Installation method of the guiding baffles in the OD

As can be seen from the results using model tests [24], the installation method for the guiding baffles has a great influence on the efficiency of oxygen transfer. The local amplification of the position and size of the guiding baffle is shown in Fig. 2. The length and width of the downstream guiding baffle are 2.31 and 6.36 cm, respectively; the vertical distance from its top edge to water surface is 4 cm, and the horizontal

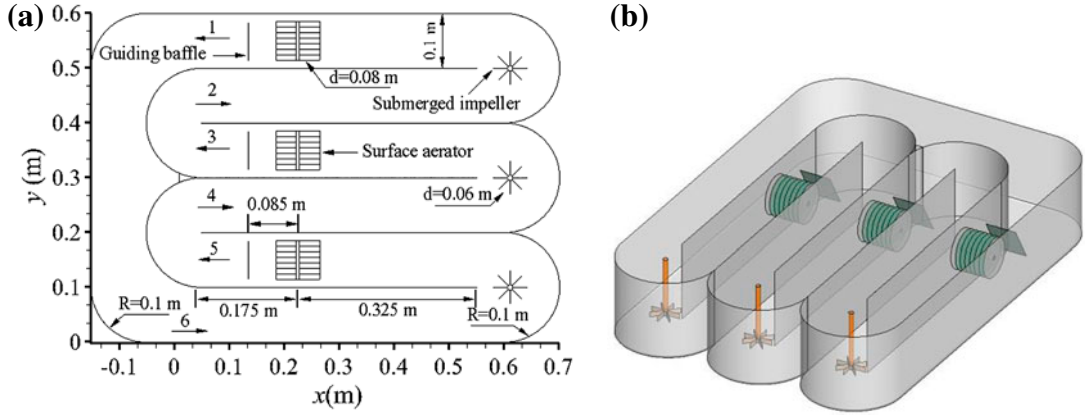

Fig. 1. (a) 2D plane and (b) 3D region of the computational domain.

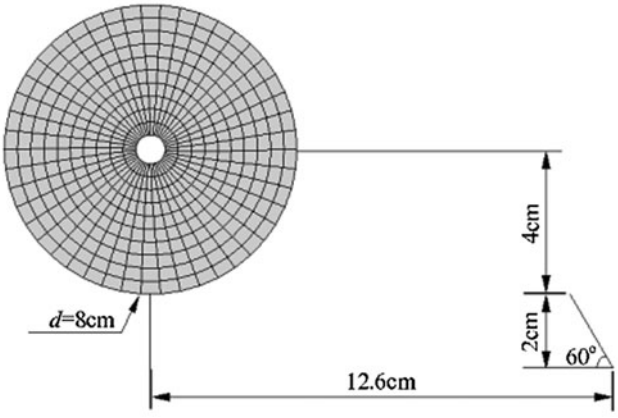

Fig. 2. Local amplification for the guiding plate.

distance from its bottom edge to the surface aerator axis is 12.6 cm; and the installation angle between the guiding baffle and the horizontal plan is 60°, as shown in Fig. 2.

3.3. Grid generation of the test model

The grid was generated by the GAMBIT software. The combination of the structured and unstructured grids was adopted. To generate a high-quality calculation grid, the thickness of disks and blades is simplified as an infinitely small one because of its very small size compared with that of the calculation region. The numbers of the elements for the OD with and without guiding baffles are 589,632 and 559,788, respectively. The grids for the OD with guiding baffles are shown in Fig. 3. Fig. 3(a)–(c) shows the 2D plane grid, 3D grid, and the grid of solid boundary of the OD, respectively.

3.4 Initial and boundary conditions

It was found that the flow inlet and outlet conditions for an OD have little influence on the flow field, so they were ignored in the numerical calculation [20]. Boundary condition at the top surface of the computational domain was given as a relative pressure zero, and that at the side walls and the bottom was given by the Wall function. The motion of submerged impellers relative to an OD was described by a MRF model with a sliding mesh method. The initial condition was given as a stationary water depth. The rotation speed of submerged impellers and surface aerators was specified.

4. Determination of the range of velocity for the test OD

To prevent sludge and pollutant deposition at the bottom of an actual OD, the designing rule for a prototype requires that the averaged cross-sectional fluid velocity, v_P, is no smaller than 0.3 m/s ($v_P \geq 0.3$ m/s) [20]. According to the designing rule and the hydraulic geometric similarity principle, the range of velocity value for the test OD can be determined. The gravity similarity theory (also named Froude number similarity theory) [25] states that the relationship between the velocity values in a prototype and its corresponding model is $\lambda_v = v_P/v_M = \lambda_L^{0.5}$, where the subscripts p and m denote prototype and model, respectively; λ_v and λ_L ($\lambda_L = 50$) are velocity and length scale ratios, respectively. Substituting the velocity value $v_P \geq 0.3$ m/s and the length scale ratio $\lambda_L = 50$ into the above formula, it can be obtained that the corresponding value should be no less than 0.00424 m/s ($v_M \geq 0.00424$ m/s) in the test model.

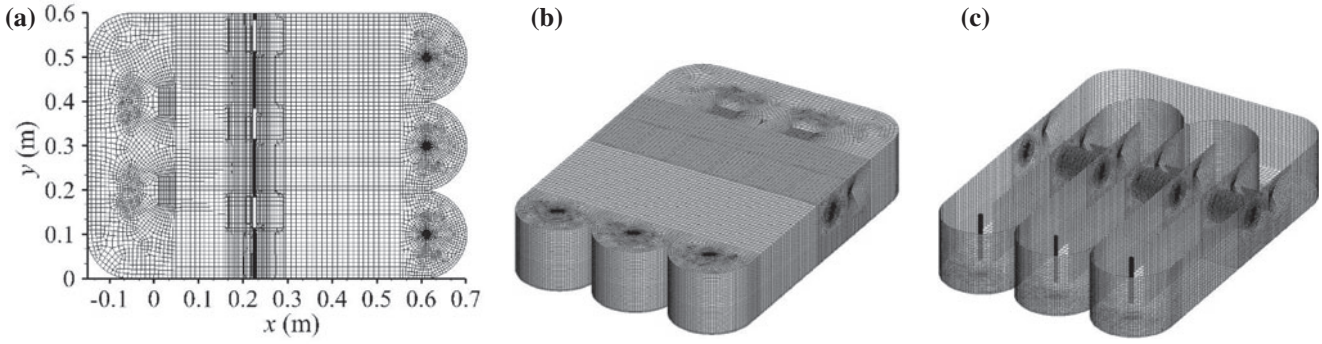

Fig. 3. Grids of the computational domain. (a) 2D plane grid, (b) 3D grid, (c) Grid of the solid boundary.

5. Result analysis and discussion

5.1. Analysis of flow field structures with and without guiding baffles

Under the two conditions (with and without guiding baffles), the simulated streamlines in the horizontal plane located at $z = 0.09$ m vertically away from the ditch bottom, were plotted in Fig. 4(a) and (b), from which one can observe that: flow velocity distributions at the bend outlets are extremely non-uniform owing to the submerged impellers, and the inertia force also makes the velocity distributions in the bends be more non-uniform, for example, in No. 1 channel, the velocity is very smaller near the straight division wall, but is much greater close to the outer wall, which leads to a recirculation zone.

Comparison of the flow structures shown in Fig. 4(a) and (b) under the two conditions (with and without guiding baffles) shows that the areas of recirculation zones after the bends are nearly the same, in another word, the guiding baffles cannot change the sizes of recirculation regions, from which it was believed that the guiding baffles do not lead to the sludge retention in the upper half ODs, also will not cause sludge deposition upstream and downstream from the guiding baffles.

Without guiding baffles, the recirculation zone appears at the left and upper corner of the outside channel, as shown in Fig. 4(a), which is the dead region for sludge retention, but it disappears with guiding baffles, as shown in Fig. 4(b).

5.2. Analysis of bottom velocity improved by guiding baffles

Fig. 5 shows the arrangement of points for the vertical lines 1–20, along which the velocity distributions will be analyzed. Here, with a constant rotation speed of submerged impellers and surface aerators, the simulated velocities in the horizontal plane located at $z = 0.02$ m vertically away from the ditch bottom were compared between the two conditions (with and without guiding baffles), as shown in Table 1.

It was seen from Table 1 that: the velocity increases obviously near the ditch bottom ($z = 0.02$ m)

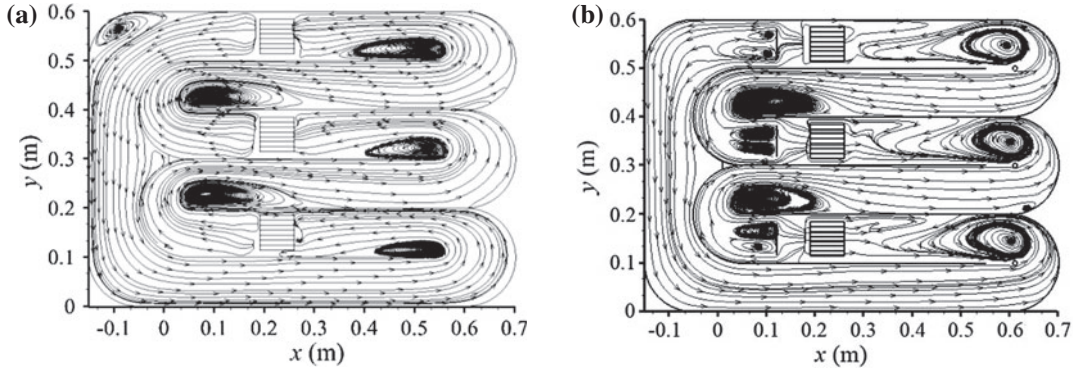

Fig. 4. Computed streamlines at $z = 0.09$ m: (a) Without guiding baffles and (b) With guiding baffles.

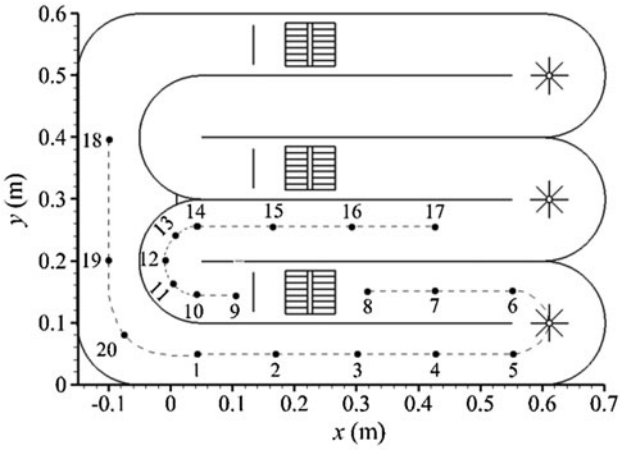

Fig. 5. Diagram of lines for vertical velocity distributions.

downstream from the surface aerators; for example, the velocity at point 9 increases from 0.046 to 0.063 m/s, so it is increased by 36.96%. The phenomenon shows that the mixture obtains energy from the surface aerator, and then is guided to the ditch bottom, which makes the bottom velocity be increased largely. The velocity values at points of 10, 11, and 12 also have confirmed that the guiding baffles can effectively increase the ditch bottom velocity.

In addition, according to Table 1, the guiding baffles can improve the flow velocities not only in a local small range after the guiding baffles, but also in the bend regions, and even in a long region after the bend regions; for example, at points 15, 16, and 17, the bottom velocities are also increased by 16.66–17.33%. This phenomenon reflects that the effect of guiding baffles on flow can still continually go through a considerable distance downstream of the surface aerators. Therefore, the guiding baffles have a significant effect on promoting the vertical mixing of flow, resulting in the uniformity improvement of velocity distributions. The effect of the guiding baffles on the velocities at points (18, 19, and 20) in the side straight channel of the OD is not obvious.

5.3. Analysis of total velocity improved by guiding baffles

In order to further display the obvious effect of guiding baffles on improving the velocity distributions in the Carrousel OD, we observed and analyzed the HV distributions along the vertical lines in Fig. 6. The positions of the vertical lines, such as the lines 3–10 and 15–17, are shown in Fig. 5. Fig. 6 was determined by the calculated HVs under the two cases (with and without guiding baffles) with the same computation boundary conditions.

Table 1
Comparison of the simulated velocities in the horizontal plane located at $z = 0.02$ m between the two conditions (with and without guiding baffles)

Points	Coordinates (x, y)	Velocities (m/s)	
		Without guide baffles	With guide baffles
1	(0.050, 0.050)	0.064	0.064
2	(0.175, 0.050)	0.070	0.070
3	(0.300, 0.050)	0.078	0.078
4	(0.425, 0.050)	0.087	0.091
5	(0.550, 0.050)	0.103	0.106
6	(0.550, 0.150)	0.043	0.101
7	(0.425, 0.150)	0.039	0.048
8	(0.325, 0.150)	0.049	0.054
9	(0.130, 0.150)	0.046	0.063
10	(0.050, 0.150)	0.047	0.051
11	(0.015, 0.165)	0.050	0.054
12	(0.000, 0.200)	0.062	0.067
13	(0.015, 0.235)	0.077	0.080
14	(0.050, 0.250)	0.082	0.089
15	(0.175, 0.250)	0.060	0.070
16	(0.300, 0.250)	0.065	0.076
17	(0.425, 0.250)	0.073	0.088
18	(–0.100, 0.400)	0.044	0.044
19	(–0.100, 0.200)	0.053	0.053
20	(–0.085, 0.065)	0.038	0.038

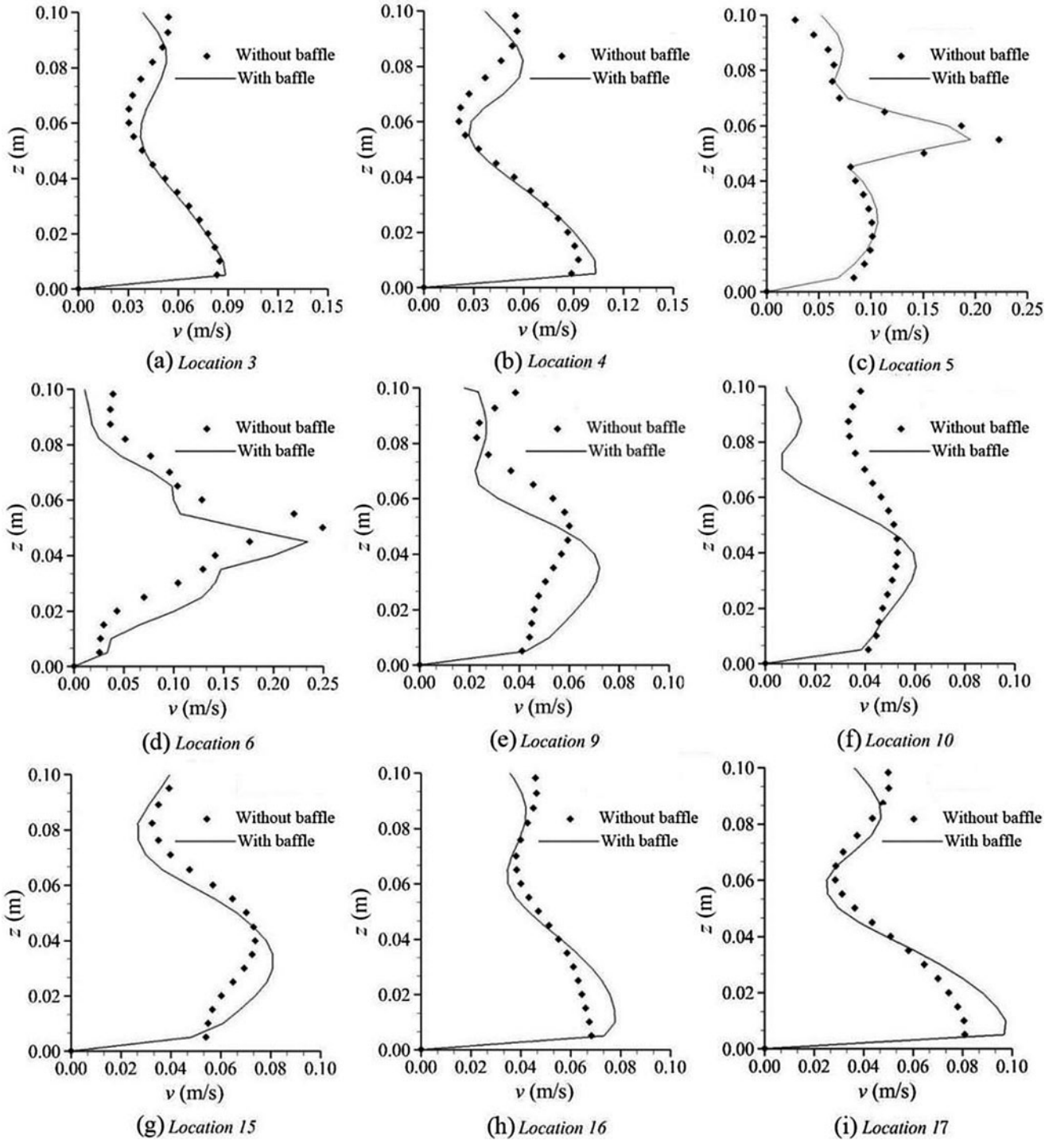

Fig. 6. Velocity distributions in vertical direction (with and without guiding baffles).

Fig. 6(a) and (b) shows the velocity distributions along the vertical lines 3 and 4 upstream from the submerged impeller in the sixth channel. When water runs through the surface aerator in the first channel, the water obtains energy from the surface aerator and is speeded. The bottom flow velocity is made larger owing to the directing effect of the guiding baffle downstream from the surface aerator. Then, the water flows to the submerged impeller at the right end of the sixth channel, and in the longer distance, the

momentum of the upper, middle, and bottom water exchanges. Therefore, when the water arrives at the vertical lines 3 and 4, the velocity of upper part of flow is little larger with guiding baffle than that without guiding baffle, but their bottom velocities are nearly the same.

Fig. 6(c) and (d) shows the flow velocity distributions along the vertical lines 5 and 6, respectively, which was affected by the submerged impeller. The abrupt increase in the velocity near the installation position (at $z = 0.055$ m) of the submerged impeller reflects the great effect of the submerged impeller on flow. The velocity distributions of the two cases with and without guiding baffles are similar. The velocities of the upper half part flow downstream of the submerged impeller are slightly decreased, but those of the lower half part flow are more increased, especially, in Fig. 6(d).

Fig. 6(e) and (f) shows the flow velocity distributions along the vertical lines 9 and 10 downstream from the surface aerator in the fifth channel, which reflect the change of flow velocities owing to the directing effect of the guiding baffles. The velocities of the upper part flow decrease obviously, and the ditch bottom velocities are significantly increased. The velocity distribution of the total flow field has been improved, which is helpful to reduce the possibility of sludge deposition due to the smaller velocity at OD bottom, and to promote the momentum exchange between the upper, middle, and lower flow in vertical direction.

Fig. 6(g)–(i) shows the velocity distributions along the vertical lines corresponding to points 15, 16, and 17. Although the vertical lines are far away from the guiding baffle and the surface aerator, the corresponding velocities at the ditch bottom are still increased, which shows that the guiding baffle not only improves the local flow near the surface aerator, but also influences the flow field structure at a great distance away from the surface aerator.

In addition, the installation of guiding baffles downstream from the surface aerators can guide the dissolved air water into the bottom of the ditch, which increases the mixture time between oxygen and water, and improve the utilization ratio of oxygen in water [3].

6. Some discussions and further study plan

Numerical simulation and experimental methods are dependent upon each other. Experiment is the main way to investigate a new basic phenomenon, taking a large amount of observation data as the foundation; still, the validation for a numerical simulation result must use the measured (in prototype or model) data. Doing numerical simulation in advance can obtain the preliminary results, which can make the corresponding experiment plan be more purposeful, and often reduce the number of tests needed by systematically doing experiments, and are much useful for the design of experimental device [20].

Here, an experimentally validated numerical tool has been used to study the effect of the installed guiding baffles downstream from the surface aerators on the flow fields in an OD. Next, further study will be done to validate the simulation model by an experimental method. An experimental model for the Carrousel OD was made of organic glass, as shown in Fig. 1. Acoustic Doppler velocimetry (ADV) will be used to measure velocities of the test model for the OD under the two working conditions with and without guiding baffles downstream from the surface aerators. The 4 points for measuring the velocities are, respectively, arranged at 0.2, 0.4, 0.5, and 0.8 of the water depth from the ditch bottom, along the 20 given vertical lines, as shown in Fig. 5. After measuring the velocity values, the measured velocity values can be compared with the calculated data, and further, the reliability of the calculation will be verified. After validating the simulation model, the CFD method can predict the flow fields in an OD with different sizes and installing positions of a guiding baffle, and the predicted results can be used to optimize the size and installing position of the guiding baffle.

7. Conclusions

The guiding baffles can be used to promote the momentum exchange between the upper, middle, and lower flow in vertical direction, by which the bottom velocity can be increased, and the local velocity distribution can be improved in an OD. The improved hydraulic feature is conducive to the elimination of sludge deposit in an OD, and improving the efficiency of water treatment.

The limitations of the guiding baffles are as follows: (1) the vertical distance from the top edge of the guiding baffle to the horizontal plane through the surface aerator axis equals to the radius of the surface aerator; (2) the installation angle from the horizontal plan to the guiding baffle is 60˚; and (3) the horizontal distance from the bottom edge of the guiding baffle to the vertical plane through the surface aerator axis is 12.6 cm in the test OD, but this value should be further determined in different ODs.

The effect of the installed guiding baffles downstream from the surface aerators on the flow

fields was numerically simulated by the experimentally validated tool in an OD. Next, further study is needed to validate the simulation results by an experimental method.

Acknowledgments

Financial support of this study was from the National Natural Science Foundation of China (grant number 51578452 and 51178391), the Scientific research project of Shaanxi Province (2014K15-03-05) and special funds for the development of characteristic key disciplines in the local university supported by the Central Financial Fund (Grant No: 106-00X101) were greatly appreciated.

Nomenclature

C_μ — model parameter in (5) with a value of 0.0845
C_1 — model parameter in (4)
C_2 — model parameter in (4) with a value of 1.68
D — diameter (m)
F — liquid volume fraction in a cell, demensionless
g_i — gravitational acceleration in i-direction, i = 1,2,3 (m/s^2)
k — turbulent kinetic energy (m^2/s^2)
p — pressure (kg/m s^2)
P_k — production term in (3) and (4)
R — radius (m)
S — parameter for computing C_1
$S_{i,j}$ — parameter for computing C_1
t — time (s)
u_i — velocity component in i-direction, i = 1,2,3 (m/s)
u_i' — fluctuating velocity component in i-direction, i = 1,2,3 (m/s)
V_c — volume of a cell (m^3)
v_m — averaged cross-sectional fluid velocity for a model (m/s)
v_p — averaged cross-sectional fluid velocity for a prototype (m/s)
V_w — volume of water inside a cell (m^3)
x_i — space coordinate in i-direction, i = 1,2,3 (m)

Greek letters

β — a constant of 0.015 for computing C_1
δ_{ij} — Kronecker function in (6), $\delta_{ij} = 1$ with $i = j$, and $\delta_{ij} = 0$ with, and with $i \neq j$
ε — kinetic energy dissipation rate (m^2/s^3)
$\tilde{\eta}$ — parameter for computing C_1
$\tilde{\eta}_0$ — a constant of 4.38 for computing C_1
λ_L — length scale ratio, demensionless
λ_v — velocity scale ratio,demensionless
μ — molecular kinematic viscosity (kg/m s)
μ_a — viscosity of air (kg/m s)
μ_t — turbulent kinematic viscosity (kg/m s)
μ_w — viscosity of water (kg/m s)
ρ — density (kg/m^3)
ρ_a — density of air (kg/m^3)
ρ_w — density of water (kg/m^3)
σ_k — model parameter in (3) with a value of 0.7197
σ_ε — model parameter in (4) with a value of 0.7197

Subscripts

a — air
c — cell
i, j — direction, i = 1, 2, and 3; j = 1, 2, and 3
L — length
M — model
P — prototype
t — turbulence
v — velocity
w — water phase

A list of abbreviations

ADV — acoustic Doppler velocimetry
CFD — computational fluid dynamics
HV — horizontal velocity
MRF — a multiple reference frame
OD — oxidation ditch
PISO — algorithm of pressure-implicit with splitting of operators
VOF — volume of fluid
WWTPs — wastewater treatment plants

References

[1] L. Fan, N. Xu, Z. Wang, H. Shi, PDA experiments and CFD simulation of a lab-scale oxidation ditch with surface aerators, Chem. Eng. Res. Des. 88 (2010) 23–33.
[2] W.M. Xie, R. Zhang, W.W. Li, B.J. Ni, F. Fang, G.P. Sheng, H.Q. Yu, J. Song, D.Z. Le, X.J. Bi, C.Q. Liu, M. Yang, Simulation and optimization of a full-scale Carrousel oxidation ditch plant for municipal wastewater treatment, Biochem. Eng. J. 56(1) (2011) 9–16.
[3] R.Y. Cao, J.Z. Fu, Measures for improving velocity distribution in oxidation ditch, China Water Waste Water. 17(2) (2001) 16–18 (in Chinese).
[4] X.M. Zhao, Hydraulic calculation of oxidation ditch, Environ. Eng. 18(2) (2000) 14–17 (in Chinese).
[5] Y. Yang, J. Yang, J. Zuo, Y. Li, S. He, X. Yang, K. Zhang, Study on two operating conditions of a full-scale oxidation ditch for optimization of energy consumption and effluent quality by using CFD model, Water Res. 45(11) (2011) 3439–3452.
[6] L. Li, J.J. He, Q. Feng, Numerical simulation of guide plate influence on flow field in the oxidation ditch, Environ. Sci. Technol. 37(2) (2014) 149–154 (in Chinese).

[7] T. Oda, T. Yano, Y. Niboshi, Development and exploitation of a multipurpose CFD tool for optimisation of microbial reaction and sludge flow, Water Sci. Techn. 53(3) (2006) 101–110.
[8] Z.L. Chen, R.W. Yang, Effect of eccentric position of guide walls on oxidation ditch performance, Environ. Eng. 28(2) (2010) 33–35 (in Chinese).
[9] S. Simon, M. Roustan, J.M. Audic, P. Chatellier, Prediction of Mean Circulation Velocity in Oxidation Ditch, Environ. Techn. 22(2) (2001) 195–204.
[10] H.H. Song, J.J. He, Z.J. Li, X.J. Zhang, Three-dimensional numerical simulation of flow fields in oxidation ditch, Chinese J. Hydrodyn. 27(2) (2012) 174–182 (in Chinese).
[11] Y.Q. Tang, J.J. He, Q.L. Liu, Numerical simulation of flow fields in an oxidation ditch of taking a submerged propeller as the power, Chinese J. Hydrodyn. 28(3) (2013) 317–323 (in Chinese).
[12] Y. Yang, Y. Wu, X. Yang, K. Zhang, J. Yang, Flow field prediction in full-scale Carrousel oxidation ditch by using computational fluid dynamics, Water Sci. Techn. 62(2) (2010) 256–265.
[13] H. Xie, J. Yang, Y. Hu, H. Zhang, Y. Yang, K. Zhang, X. Zhu, Y. Li, C. Yang, Simulation of flow field and sludge settling in a full-scale oxidation ditch by using a two-phase flow CFD model, Chem. Eng. Sci. 109 (2014) 296–305.
[14] L. Lei, J. Ni, Three-dimensional three-phase model for simulation of hydrodynamics, oxygen mass transfer, carbon oxidation, nitrification and denitrification in an oxidation ditch, Water Res. 53 (2014) 200–214.
[15] M. Fouad, A. El-Morsy, Sludge accumulation pattern inside oxidation ditch case study, Water Sci. Techn. 69(12) (2014) 2468–2475.
[16] A. Abusam, K.J. Keesman, H. Spanjers, G. van Straten, K. Meinema, Effect of oxidation ditch horizontal velocity on the nitrogen removal process, European Water Management Online, Official Publication of the European Water Association (EWAEWA), 2002, pp. 1–9.
[17] Metcalf & Eddy, Wastewater Engineering (Treatment, Disposal, & Reuse). fourth ed., McGraw-Hill Book Co., 2003 pp. 776–778.
[18] S. Gillot, S. Capela, A. Heduit, Effect of horizontal flow on oxygen surfactants transfer in clean water and in clean water with surfactants, Water Res. 34(2) (2000) 678–683.
[19] M. Gresch, M. Armbruster, D. Braun, W. Gujer, Effects aeration patterns on the flow field in wastewater aeration tanks, Water Res. 45 (2010) 810–818.
[20] W. Wei, Y. Liu, B. Lv, Numerical simulation of optimal submergence depth of impellers in an oxidation ditch, Desalin. Water Treat. Pub. online 13 (Mar 2015) 1–8, doi: 10.1080/19443994.2015.1021840.
[21] W.L. Wei, H.C. Dai, Turbulence Model Theory and Engineering Applications, first ed., Shanxi Science and Technology Press. Xi'an City, 2006 (in Chinese).
[22] V. Yakhot, S.A. Orzag, Renormalization group analysis of turbulence: Basic theory, J. Sci. Comput. 1 (1986) 3–11.
[23] V. Yakhot, S.A. Orszag, S. Thangam, T.B. Gatski, C.G. Speziale, Development of turbulence models for shear flows by a double expansion technique, Phy. Fluids A 4(7) (1992) 1510–1520.
[24] F.W. Dang, S.J. Zhang, The application of guide plate in the productive oxidation ditch, Liaoning Urban Rural Environ. Sci. Technol. 25(5) (2005) 29–31 (in Chinese).
[25] E. Jonhn Finnemore, B. Joseph Franzini, Fluid Mechanics with Engineering Applications, tenth ed., McGraw-Hill, 2002.